RETRIEVING DRY SNOW DEPTH BASED ON CO-POLARIZED PHASE DIFFERENCE OF X-BAND RADAR IMAGE

Pengfeng Xiao, Senior Member, IEEE, Yue Zhuo, Xueliang Zhang, Xuezhi Feng, Yina Song

Department of Geographic Information Science, School of Geography and Ocean Science, Nanjing University, China

ABSTRACT

Snow depth is of great significance for hydrological simulation and climate research. The Co-polarized Phase Difference (CPD) between VV and HH polarization of Synthetic Aperture Radar (SAR) systems shows a significant dependence on the depth of fresh snow. This study develops a retrieval model of dry snow depth based on CPD of X-band SAR image in cropland and barren of Northwest China. First, the forward model is presented and its sensitivity to ice grain shape, snow density, incidence angle, and radar wavelength is analyzed. Second, the snow depth retrieval model is developed and the optimal filter window size is determined. Finally, the dependence of the retrieval model on different underlying surface type, snow density, and terrain is evaluated. The study reveals the influence factors of the CPD model and provides valuable spatial distribution of snow depth for water resource management.

Index Terms—snow depth, synthetic aperture radar, co-polarized phase difference, X-band

1. INTRODUCTION

Snow depth distribution is an important parameter for water management, avalanche forecast, and climate research [1]. Active radar sensors, especially Synthetic Aperture Radar (SAR) systems show a sensitivity to snow volume with resolution on meter scale [2]. The phase difference between the co-polarized terms of scattering matrix, S_{VV} and S_{HH}, was found to be related to snowpack features including anisotropy, wetness, density, and particle size [3]. Moreover, this Co-polarized Phase Difference (CPD) displayed an increasing trend with snow depth [4]. Recently, the work [2] presented a theoretical relationship between the microstructure of snow and the CPD [5], and relates the CPD theoretically and empirically to the snow depth of fresh snow [2]. The test site is located in northern Finland and the dominant land cover types are bogs and peat, but the applications of the model in other underlying surface types have not been explored.

In this study, we develop the CPD-based snow depth retrieval model in cropland and barren of Northwest China, and reveal its influence factors including filter window size, underlying surface type, snow density, and terrain. The findings will contribute to the application of CPD model and will provide valuable spatial distribution of snow depth for water resource management.

2. STUDY AREA

The study area is in Altay, Xinjiang Province, China. As shown in Figure 1, Altay City is located in the southwest pediment of the Altay Mountains, which are mountains range in Central and East Asia, where China, Russia, Mongolia, and Kazakhstan come together, and where the rivers Irtysh and Ob have their headwaters. The study area is in the watershed of Kelan River, a head branch of Irtysh River.

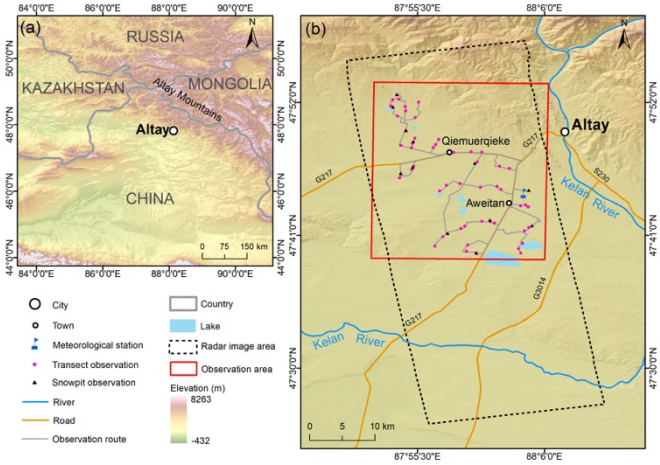

Fig. 1. Study area in Altay, Xinjiang Province, China. (a) illustrates the location of Altay City, and (b) shows the radar image area, the observation area, and the distribution of observation points.

Altay is often called "Snow City", as the surrounding region is well-known for its deep snowpack (~50 cm) and its spring snowmelt flood in Northwest China. The southwest piedmont of Altay Mountains faces the cold and wet westerly wind from the Atlantic Ocean in winter, bringing in the heavy snowfall. The deep snowpack in the mountains provides the vital water supply to the Irtysh River, consisting of almost 50% of total river runoff [6].

3. DATA

3.1. Satellite Data

A X-band TerraSAR-X radar image with HH and VV polarization in StripMap model is used to calculate the CPD (see Fig. 1). It is in descending orbit and right side looking. The acquisition time is 17:58, 18 January 2018 in local time. The incidence angle is 42.3253°. The range and azimuth resolution is 1.36 m and 2.40 m, respectively.

In addition, the Shuttle Radar Topography Mission (SRTM) Digital Elevation Model (DEM) data with 30-m resolution is used to calculate local incidence angle. The GlobeLand30 land cover data with 30-m resolution is used to indicate underlying surface type.

3.2. Field Survey Data

The field work was implemented in the daytime of 18 and 19 January because the satellite observation is in the night of 18 January. The observation area is in the north part of the radar image (see Fig. 1), containing the Altay Meteorological Station. We designed a strategy integrating transact and snowpit observations. The former measured snow depth, snow density, and snow layer temperature to obtain a large amount of snow properties for fitting and validation of inversion model. The latter measured snow layer dielectric constant, snow layer humidity, and snow grain size to tell whether the snow state is applicable to CPD model.

We obtained measured data of 51 transact samples and 12 snowpit samples. The results indicate that the measured data meet the conditions of CPD model as shown in Fig. 2: (1) the snow depth is concentrated at 13–16 cm; (2) the snow density is concentrated at 0.13–0.17 g/cm^3; (3) the average snow water equivalent (SWE) is 2.19 cm; (4) the underlying surface type of the 51 samples is mainly cropland (33 samples) and barren (16 samples); and (5) the local incidence angles of 51 samples in SAR images are distributed in 37.28–45.08°, and concentrated at 42.3°.

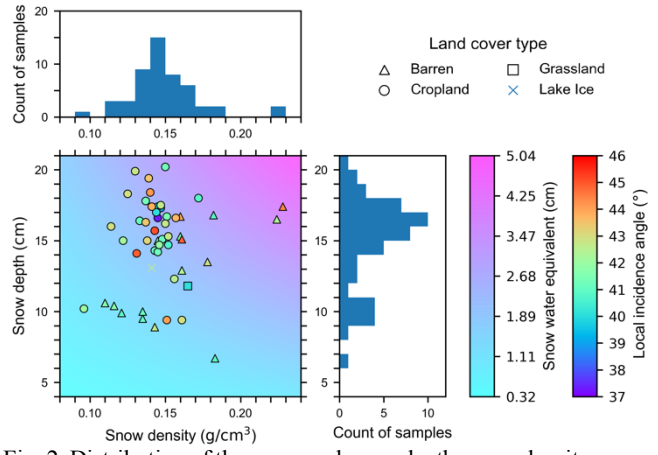

Fig. 2. Distribution of the measured snow depth, snow density, snow water equivalent, local incidence angle, and underlying land cover types.

4. METHODOLOGY

4.1. Forward Model

Fresh snow accumulates as a randomly structured medium composed of ice and air. The fresh snow volume is compressed by its own weight. A few days to weeks later, recrystallization forms first spherical and later vertically extended ice grains, which increase in size by time: (1) random; (2) horizontally aligned; (3) isotropic; and (4) vertically aligned [7].

A single spheroidal particle can be characterized by three orthogonal dipoles with lengths a_x, a_y and a_z in the axes of x-, y-, and z-axes. The horizontal-to-vertical axes ratio a_x/a_z defines the shape of the spheroid, assuming that $a_x = a_y$. $a_x/a_z > 1$ refer to horizontally oriented oblates. Contrarily, $a_x/a_z < 1$ indicate vertically oriented prolates. By fixing a particle shape, the three depolarization factors N_i with $i \in \{x, y, z\}$ of a single spheroid can be computed by [8]:

$$N_i = \frac{a_x a_y a_z}{2} \int_0^\infty \frac{ds}{(s+a_i^2)\sqrt{(s+a_x^2)(s+a_y^2)(s+a_z^2)}} \quad (1)$$

Considering air as a medium of permittivity ε_{air} populated by aligned spheroidal ice particles of permittivity ε_{air}, the effective permittivity of the mixture is anisotropic. Along the three main directions, it can be written as [2]:

$$\varepsilon_{\text{eff},i} = \varepsilon_{\text{air}} + \mu \cdot \varepsilon_{\text{air}} \cdot \frac{\varepsilon_{\text{ice}} - \varepsilon_{\text{air}}}{\varepsilon_{\text{air}} + (1-\mu) N_i (\varepsilon_{\text{ice}} - \varepsilon_{\text{air}})} \quad (2)$$

where μ is particle volume fraction, which is based on the density of snow, ice, and air. The elements of the effective permittivity are projected onto the h- and v-axes of the radar reference frame to include the dependency on the incidence angle θ. The refraction indices n_H and n_V follow from the relation $\varepsilon = n^2$. Dry snow is considered as a nonabsorbing medium, thus no imaginary parts appear in n [2].

$$n_H^2 = \varepsilon_{\text{eff},H} = \varepsilon_{\text{eff},x} \quad (3)$$

$$n_V^2 = \varepsilon_{\text{eff},V} = \varepsilon_{\text{eff},y} \cdot \cos^2\theta + \varepsilon_{\text{eff},z} \cdot \sin^2\theta \quad (4)$$

$$\Delta n = n_V - n_H \quad (5)$$

The CPD is then obtained with the refraction difference Δn, the snow depth SD, and the wavelength λ of the SAR system [2].

$$\phi = \frac{4\pi}{\lambda} SD \cdot \Delta n \quad (6)$$

We analyze the CPD changes with each parameter in different snow depth and reveal that the CPD is: (1) only sensitive to fresh snow with $a_x/a_z > 1$; (2) more sensitive to snow with high density (0.1–0.5 g/cm^3); (3) more sensitive to great incidence angle ($0 < \lambda < 90°$); and (4) more sensitive to microwave with short wavelength (Fig. 3).

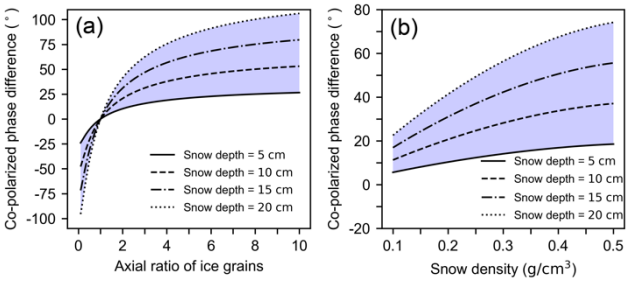

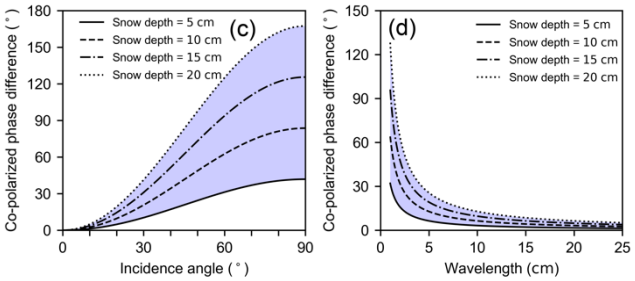

Fig. 3. Sensitivity of CPD to snow depth under different axial ratio of ice grains (a), snow density (b), incidence angle (c), and wavelength (d) of SAR systems.

4.2. Retrieval Model

The remotely sensed CPD is extracted from the polarimetric coherence $\tilde{\gamma_c}$:

$$\tilde{\gamma_c} = \gamma_c \cdot e^{i\phi_c} = \frac{\langle S_{VV} S_{HH}^* \rangle}{\sqrt{\langle |S_{VV}|^2 \rangle \cdot \langle |S_{HH}|^2 \rangle}} \quad (7)$$

where γ_c is coherence coefficient; ϕ_c is CPD; S_{VV} and S_{HH} are Single Look Complex (SLC) values of VV and HH polarization, respectively; $*$ refers to complex conjugate; and $\langle \cdot \rangle$ refers to a 2-D Gaussian filter to remove speckle noise.

The SLC images are geocoded by solving the range, Dopper and ellipsoid equation including the SRTM DEM. The CPD is calculated in radar coordinates and then transformed into WGS84 coordinates.

According to the forward model of CPD, there is a linear fit relation between CPD and snow depth, which is the retrieval model:

$$CPD = a \times SD + b \quad (8)$$

where CPD is calculated using SAR image; SD is field measured snow depth; and a and b are fit coefficients. a refers to CPD change caused by unit snow depth, $a > 0$ for fresh snow. b influences by horizontal-to-vertical axes ratio, snow density, incidence angle, and wavelength.

4.3. Validation Method

We adopt cross validation to evaluate the snow depth retrieval model, because the limited 51 measured samples are used not only as validation samples but also as fitting samples. There are three cross-validation methods: hold-out, K-fold, and leave-P-out. We use the leave-P-out cross validation method, as it is exhaustive in the sense that it needs to train and validate the model for all possible combinations. Let P = 3, calculation times are $C_{51}^3 = 20825$. In each time using 48 samples to fit and 3 samples to validate the model. R^2 of fitting and validation reflects the level of linear relation between CPD and measured snow depth.

5. RESULTS

5.1. Snow Depth Retrieval Results

The experiment reveals that the remotely sensed CPD is seriously affected by the filter window size, thus we fit and validate with every filter window size using the leave-P-out method (Fig. 4). The results show that the optimal retrieval result of snow depth is appeared with filter window size 69 pixels. The fit model of CPD and the retrieval model of snow depth respectively are:

$$CPD = 0.22 \times SD - 2.98 \quad (9)$$

$$SD = 4.55 \times CPD + 13.55 \quad (10)$$

This means the CPD value caused by every 1 cm depth snow is 0.22 °. The validation accuracy is R^2 = 0.50 and RMSE = 3.18 cm.

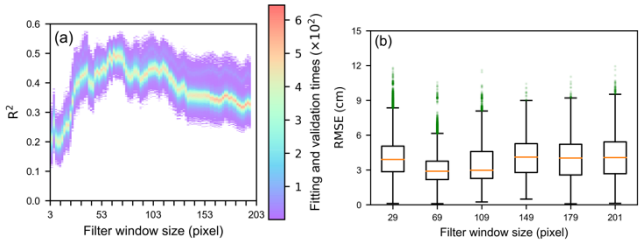

Fig. 4. Validation R^2 and RMSE calculated 20825 times in each filter window size.

The spatial distribution of retrieved snow depth is shown in Fig. 5. The snow-destroyed area (residential), snow-cleaned area (roads and airport), frozen area (water), and complex scattering area (forest) are masked before the retrieval. It is shown that the retrieved snow depth increases from the south (plain) to the north (piedmont). The minimum value is in the southwest, gobi area, and the maximum value is in the north, along Altay Mountains. The average snow depth is ~16 cm, where the dominant underlying surface type is cropland and barren.

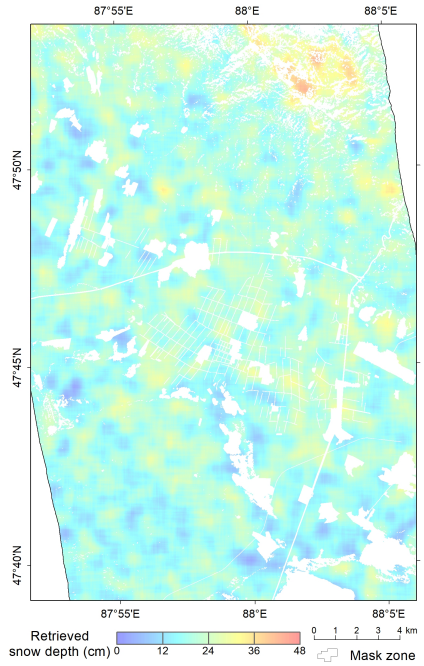

Fig. 5. Retrieved snow depth of the study area with the optimal filter window size.

5.2. Influence of Underlying Surface Type

Different underlying surface type has different scatting properties, this changes the proportion of CPD caused by snow to the total CPD. We build two models for the cropland and barren separately, then the validation R^2 reaches 0.59 and 0.85 for cropland and barren in optimal filter window size 125 and 55 pixels, respectively (Fig. 6).

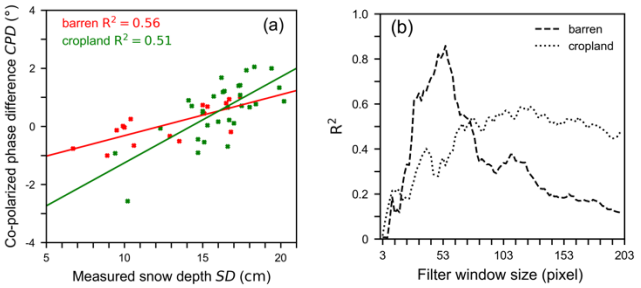

Fig. 6. Fit of measured SD and CPD of two types of underlying surface, i.e. barren and cropland (a), and its validation R^2 with different filter window size (b).

5.3. Influence of Snow Density

The snow density decides the particle volume fraction when calculating CPD, then influences the snow depth retrieval. We build four models according to the range of measured snow density, then the validation R^2 reaches 0.88, 0.46, 0.85, and 0.96 for the four models in optimal filter window size 75, 185, 117, and 69 pixels, respectively (Fig. 7).

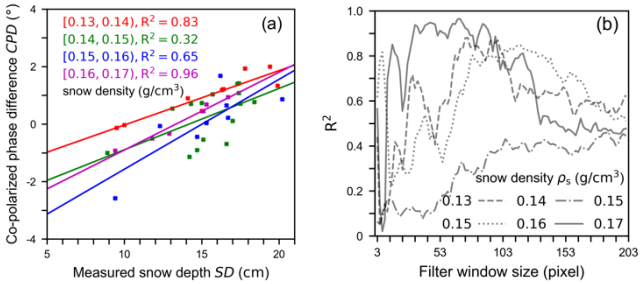

Fig. 7. Fit of measured SD and CPD of four types of snow density (a) and its validation R^2 with different filter window size (b).

5.4. Influence of Terrain

The terrain influences local incidence angle, the retrieval errors will increase if neglect the difference of local incidence angle. We build three models according to the range of local incidence angles, then the validation R^2 reaches 0.50, 0.72, and 0.91 for the four models in optimal filter window size 41, 79, and 69 pixels, respectively (Fig. 8).

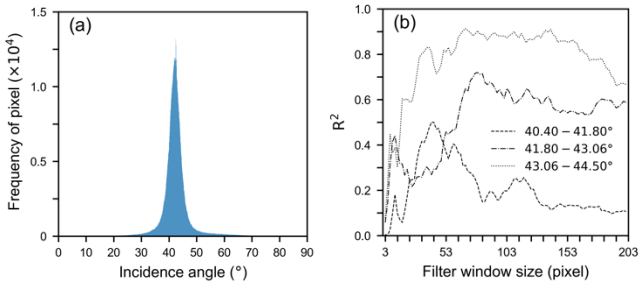

Fig. 8. Histogram of the local incidence angles (a) and the validation R^2 of the three types of local incidence angle with different filter window size (b).

6. CONCLUSIONS

This study develops a retrieval model of dry snow depth based on CPD of X-band SAR image in cropland and barren of Northwest China. The sensitivity analysis of the forward model reveals that the CPD is sensitive to fresh snow, high density, great incidence angle, and short wavelength. The influence analysis of the retrieval model on different underlying surface type, snow density, and terrain shows that the model is applicable to dry snow depth retrieval in cropland and barren, this provides valuable spatial distribution of snow depth for water resource management.

REFERENCES

[1] K. J. Bormann, R. D. Brown, C. Derksen, and T. H. Painter, "Estimating snow-cover trends from space," *Nat. Clim. Change*, vol. 8, no. 11, pp. 924–928, Nov. 2018.

[2] S. Leinss, G. Parrella, and I. Hajnsek, "Snow Height Determination by Polarimetric Phase Differences in X-Band SAR Data," *IEEE J. Sel. Top. Appl. Earth Obs. Remote Sens.*, vol. 7, no. 9, pp. 3794–3810, Sep. 2014.

[3] P. S. Chang, J. B. Mead, E. J. Knapp, G. A. Sadowy, R. E. Davis, and R. E. McIntosh, "Polarimetric backscatter from fresh and metamorphic snowcover at millimeter wavelengths," *IEEE Trans. Antennas Propag.*, vol. 44, no. 1, pp. 58–73, Jan. 1996.

[4] J. P. S. Gill, J. J. Yackel, T. Geldsetzer, and M. C. Fuller, "Sensitivity of C-band synthetic aperture radar polarimetric parameters to snow thickness over landfast smooth first-year sea ice," *Remote Sens. Environ.*, vol. 166, pp. 34–49, Sep. 2015.

[5] S. Leinss, H. Löwe, M. Proksch, J. Lemmetyinen, A. Wiesmann, and I. Hajnsek, "Anisotropy of seasonal snow measured by polarimetric phase differences in radar time series," *The Cryosphere*, p. 27, 2016.

[6] Y. Shen, G. Wang, Q. Wu, N. Wang, W. Mao, and H. Su, "Responses to climate warming of hydrological processes in the upper Kelan River in the Altay Mountains, Xinjiang, China," *Sci. Cold Arid Reg.*, p. 13, 2010.

[7] M. Schneebeli and S. A. Sokratov, "Tomography of temperature gradient metamorphism of snow and associated changes in heat conductivity," *Hydrol. Process.*, vol. 18, no. 18, pp. 3655–3665, Dec. 2004.

[8] A. Sihvola, "Mixing Rules with Complex Dielectric Coefficients," *Subsurf. Sens. Technol. Appl.*, vol. 1, no. 4, pp. 393–415, Oct. 2000.